Automatica 117 (2020) 108956

Contents lists available at ScienceDirect

Automatica

journal homepage: www.elsevier.com/locate/automatica

Integrated supervised adaptive control for the more Electric Aircraft ☆

Alberto Cavallo *, Giacomo Canciello, Antonio Russo

Dipartimento di Ingegneria, Università degli Studi della Campania "L. Vanvitelli", 81031 Aversa (CE), Italy

ARTICLE INFO

Article history:
Received 17 June 2019
Received in revised form 22 November 2019
Accepted 3 March 2020
Available online 4 April 2020

Keywords:
Supervisory control
Nonlinear control
Stability domains
Adaptive control
Robust control
Aircraft control

ABSTRACT

The innovative concept of Electric Aircraft is a challenging topic involving different control objectives. For instance, it becomes possible to reduce the size and the weight of the generator by using the battery as an auxiliary generator in some operation phases. However, control strategies with different objectives can be conflicting and they can produce undesirable effects, even instability. For this reason an integrated control design approach is needed, such that stability can be guaranteed in any configuration. In other words, the design of the supervisory controller must be interlaced with that of low-level controllers. Moreover, uncertainties and noisy signals require robust control techniques and the use of adaptiveness in the control algorithm. In this paper, the use of a new adaptive sliding manifold design is proposed for increase robustness against uncertainties and noisy signals, together with a new supervisor exploiting the estimate of the region of attraction of the control laws. A bidirectional voltage converter aiming at recharging batteries and to use the battery to withstand generator overloads is addressed. Detailed and rigorous stability proofs are given for any control configuration, including the switching phases among different control objectives. Effectiveness of the proposed strategies is shown by using a detailed simulator including switching electronic components.

1. Introduction

Control of electric power systems is one of the most known applications of Automatic Control theory. The traditional approach is to consider models of the devices linearised around their equilibrium working point and to resort to the theory of control for linear time-invariant systems to design the controller, or simply to employ standard PID (Proportional–Integral–Derivative) controllers. However, this approach suffers from the well-known drawbacks of linearisation, mainly that only local results can be stated, possibly in narrow regions of the space in which the system state takes its values. Nonlinear control strategies have been proposed to alleviate the above problem, especially by resorting to the SMC (Sliding Mode Control) approach (Utkin, 1992, 1993; Utkin, Guldner, & Shi, 2009; Young, Utkin, & Ozguner, 1999) or using backstepping methods (Fu, Zhao, & Dimirovski, 2006; Sun, Zhao, & Dimirovski, 2009). Basically, SMC consists in defining a suitable manifold such that as the system state is constrained to belong to this manifold, the control objective is achieved. The dynamic evolution of the system when sliding on the manifold is determined by the *reduced order system*, that is the closed-loop system when the so-called *equivalent control* is applied (see (Utkin, 1977) for a definition of the terms). Since the classic SMC produces a discontinuous control, this seems to be the most natural control approach for power systems, where the flow of power is modulated by suitably turning on and off electronic switches (Biel & Fossas, 2004; Sira-Ramírez, 2015; Sira-Ramírez & Ilic, 1988; Utkin, 1993). Traditionally, one of the main concern in the direct implementations of SMC is that the control signal has not a fixed switching frequency. This has been solved either by resorting to "regularised" versions of the SMC or by using more recent Second Order SMC (SOSMC) (Bartolini, Ferrara, & Usai, 1997; Bartolini, Ferrara, Utkin, & Zolezzi, 1997; Cucuzzella, Rosti, Cavallo, & Ferrara, 2017; Levant, 2003; Sabanovic, Fridman, & Spurgeon, 2004), that produce a continuous control, and then employing a standard PWM (Pulse Width Modulation) device operating at fixed switching frequency. In spite of the above concern, however, some direct implementations of SMC, i.e., with the controller driving directly the power switches, both in continuous and discrete time, have been proposed (Lopez, Garcia De Vicuna, Castilla, Matas, & Lopez, 1999; Sira-Ramírez & Silva-Ortigoza, 2006; Yang, Zhong, Kiratipongvoot, Tan, & Hui, 2018), showing the superiority of the direct SMC over the implementation through PWM.

Another point to be addressed is the selection of the sliding surface. Indeed, direct formulation of the control objective in

☆ This paper has been partially supported by Clean-Sky2 grant Programme: H2020-CS2-CFP04-2016-02 JTI-CS2-2016-CFP04-REG-01-08, Proposal: 755485 ESTEEM. The material in this paper was not presented at any conference. This paper was recommended for publication in revised form by Associate Editor Peng Shi under the direction of Editor Thomas Parisini.
* Corresponding author.
E-mail addresses: alberto.cavallo@unicampania.it (A. Cavallo), giacomo.canciello@unicampania.it (G. Canciello), antonio.russo1@unicampania.it (A. Russo).

https://doi.org/10.1016/j.automatica.2020.108956
0005-1098/

the sliding function, e.g., definition of a reference current or voltage to be tracked, usually leads to a nonlinear reduced order system (Cavallo, Canciello, & Guida, 2017; Sira-Ramírez, 2015). Recently, the authors have proposed a suitable selection of the sliding function such that the system in sliding mode behaves as a linear system (Cavallo, Canciello, & Guida, 2018). The limitation of this approach is that at least a good estimate of the (uncertain) load is required, and this has been achieved in Cavallo, Canciello, and Guida (2018) by using a Levant differentiator (Levant, 1998). As an alternative, in this paper a new approach based on an adaptive version of the sliding surface is proposed. Adaptive control is not new SMC application (Incremona, Cucuzzella, & Ferrara, 2016; Plestan, Shtessel, Brégeault, & Poznyak, 2010; Utkin & Poznyak, 2013). However, usually the adaptation strategy adapts the magnitude of the control action in such a way to ensure stability of the closed-loop. In this paper, on the other side, the adaptivity of the sliding manifold itself is addressed. Adaptive sliding functions (and manifolds) have been presented in Durmaz, Özgören, and Salamci (2012) and Hušek (2016). While the former is based on the resolution of the State-Dependent Riccati Equations (SDRE) to compute the slope and the offset of the sliding manifold, the latter considers an algorithmic procedure to shift or rotate the sliding manifold. In this paper, adaptation of the sliding manifold is achieved through estimation of a scalar parameter until the steady-state values of the reduced order system fulfil the control objectives.

Currently, in innovative applications it is usual for a control system to switch among different tasks when different external conditions change, possibly changing equilibrium points, and even changing control law. Moreover, as external disturbances affect the controlled plant it can be better to emphasise a control objective over another, possibly automatically switching among different controllers. It is clear that the more sophisticated the objective, the more complex must be the control theory to deal with them. The focus of control scientist in the last decade on switched systems and formalised supervisory strategies is directed towards this objective, even in the presence of faulty actuators (Li, Zhao, & Dimirovski, 2011) or constant power loads (Cavallo, Canciello, & Russo, 2018a).

A subtle issue appears in the case of a supervisory control action autonomously switching among different stable configurations, e.g., due to changing control objective. In this case, counterexamples have been found showing that switching among stable configurations can result into overall instability (Branicky, 1998). In the case of switched linear systems, an interesting solution aimed at reducing the undesired transient behaviours induced by switching is presented in Zhao, Ma, and Zhao (2018), Zhao, Zhao, Fu, and Dimirovski (2019) where bumpless transfer control techniques have been adopted. However this approach does not easily fit the considered case of supervisory control switching among nonlinear systems. The above drawbacks can be explicitly dealt with by co-designing high-level and low-level control. Specifically, low-level controllers that fulfil standard requirements (e.g., closed-loop stability, robustness) are designed, but also an estimate of the region of attraction of the control strategy is produced. This is helpful for the high-level control, that must reformulate control objectives so as to adapt their action to the current condition of the controlled system, with reference to the regions of attraction mentioned above. A new supervisory strategy is proposed ensuring that the state of the controlled systems never exists suitably defined invariant sets, so that stability is never lost.

The above ideas can be adopted to solve challenges in the framework of the More Electric Aircraft (MEA) (Aeroval Inc., 2020). One of the objectives of the MEA is the replacement of hydraulic and pneumatic devices with their electric counterpart. The increased number of electric and electronic devices onboard calls for the need of automated control algorithms aimed at achieving specific control goals. A multi-objective problem for the MEA involving the control of a bidirectional DC–DC Converter, specifically a BBCU (Buck-Boost Converter Unit), has been addressed by the authors (Cavallo, Canciello, & Russo, 2018b; Cavallo, Russo, & Canciello, 2019). Specifically, the aircraft power grid can be modelled as a simple two-busbars system (Cavallo, Guida, Buonanno, & Sparaco, 2015; Tooley, 2009), one high voltage (HV) DC bus at 270V and a low voltage (LV) DC bus at 28V, with a DC–DC bidirectional converter in between. The HV bus is energised by a starter-generator followed by a rectifier. On the HV side all the "heavy" loads are present (e.g., anti-icing, de-icing or electromechanic actuators (Cavallo, Russo, & Canciello, 2019; Russo & Cavallo, 2020)). On the LV side a battery is located, for avionics and emergency conditions. In normal operating conditions the battery is charged by the generator (so the battery is a further load for the generator). Since generator sizing is based on its capability to withstand large loads for more than 5s, (the so-called 5s-5 min capability (Cavallo et al., 2017) the idea is to use the battery to help the generator in the case of overload, so as to reduce generator sizing (and weight). It is clear from the above discussion that the battery must be able to supply power to the HV size within 5s from the request, so as to comply with the 5s-5 min constraint.

The rest of the paper is organised as follows. Section 2 presents the model of the bidirectional converter to control, along with some physical considerations. Section 3 is the core of the paper and presents the mathematical results. It is split into three different subsections, showing the uniform stability of the controlled system, the stability of the adaptive control laws with different control objectives, and the supervisory control, respectively. All the strategies are presented with a single, integrated design approach taking into account an estimate of the Regions of Attraction of the control as a vital part of the design. Section 4 presents a possible implementation of the integrated strategy discussed in Section 3, along with detailed simulation to test the effectiveness of the proposed. Finally, some conclusions are presented in Section 5.

2. BBCU Model

The BBCU bidirectional converted considered in this paper is shown in Fig. 1. This circuit is representative of the HV and LV buses on-board aircraft. As stated in the Introduction, the HV side voltage source is a three-phases generator undergoing rectification which is here schematically represented as an ideal DC voltage generator E_H and its internal resistance R_H. Also the battery on the LV side is represented by an ideal voltage generator E_L and its internal resistance R_L. The bidirectional converter employs an inductor L and two capacitors, one for each side, C_H and C_L for the HV and the LV side, respectively. The circuit modulates power due to two switches, Q_1 and Q_2, which are controlled by an ON/OFF synchronised signal. Since only active power is of interest for this application, the load can be modelled as a resistor R_D with a piece-wise constant resistance value. Therefore, a load variation will be simulated by a variation of the circuit resistance R_D.

The circuit equations are easily derived for both configurations (Q_1 OFF, Q_2 ON) and (Q_1 ON, Q_2 OFF) and can be written in a compact way as

$$\dot{x}_1 = -\frac{1}{L}x_3 + \frac{1}{L}x_2 u \tag{1}$$

$$\dot{x}_2 = -\alpha x_2 - \frac{1}{C_H}x_1 u + \beta_H \tag{2}$$

$$\dot{x}_3 = \frac{1}{C_L}x_1 - \frac{1}{R_L C_L}x_3 + \beta_L \tag{3}$$

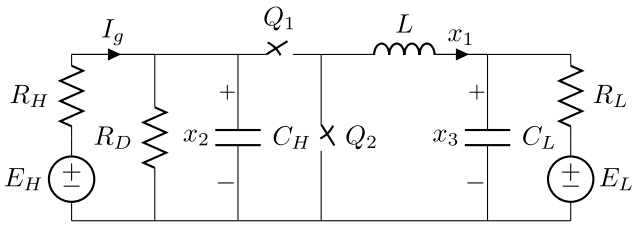

Fig. 1. Bidirectional Buck-Boost converter schematic.

where

$$\alpha = \frac{1}{R_{DH} C_H}, R_{DH} = \frac{R_D R_H}{R_D + R_H}, \beta_i = \frac{E_i}{R_i C_i}, i = H, L \tag{4}$$

x_1 is the current flowing through the inductor L, x_2 is the voltage across the capacitor C_H on the HV bus side, x_3 is the voltage across the capacitor C_L on the LV bus side, and the control $u \in \{0, 1\}$ is a binary variable defining the two configurations. Note that R_{DH} is physically the value of the resistance resulting from the parallel connection of R_D and R_H. Finally, we assume that $E_H > E_L$ and that the resistor R_H is small enough so that

$$E_H > (1 + R_H/R_D)\, E_L \tag{5}$$

Physically this requirement is very reasonable, since usually $R_H/R_D \ll 1$.

3. BBCU Control

The control of the BBCU is designed in a hierarchical manner. A low-level control layer is designed in order to accomplish proper current tracking capabilities while a high-level control layer is responsible for the selection of the proper BBCU operating modality according to a prescribed functional policy. Preliminarily, we point out a structural property of the system under consideration. Then we will discuss the control strategies.

3.1. Uniform stability of the BBCU

In this Section we show that there is no loss of generality in assuming the BBCU to operate in a bounded region in the variables state space. To formally show this statement, we present the following Lemma.

Lemma 1 (*Uniform Stability*). *Consider the system (1)–(3) and let u be any control $u \in \mathcal{L}_\infty$. Then the system (1)–(3) is uniformly stable.*

Proof. Consider a nonzero solution $\xi = \xi(t)$ of the system (1)–(3) for a bounded $u = u(t)$. Using the change of variables

$$y(t) = x(t) - \xi(t) \tag{6}$$

the translated system can be written as

$$\dot{y}_1 = -\frac{1}{L} y_3 + \frac{1}{L} y_2 u(t) \tag{7}$$

$$\dot{y}_2 = -\alpha y_2 - \frac{1}{C_H} y_1 u(t) \tag{8}$$

$$\dot{y}_3 = \frac{1}{C_L} y_1 - \frac{1}{R_L C_L} y_3 \tag{9}$$

Note that, due to the assumption $u \in \mathcal{L}_\infty$, the right-hand side of (7)–(9) is locally Lipschitz in y on a domain $D \subset \mathbb{R}^n$. Now, consider the Lyapunov function

$$V(y) = \frac{1}{2}\left(L y_1^2 + C_H y_2^2 + C_L y_3^2\right) \tag{10}$$

whose time derivative along the trajectory of the system is

$$\dot{V}(y) = -\frac{1}{R_{DH}} y_2^2 - \frac{1}{R_L} y_3^2 \leq 0. \tag{11}$$

Thus, using Khalil (2002, Theorem 4.8), with the two quadratic functions $W_1(y) = 1/2 \min\{L, C_H, C_L\}\|y\|^2$, $W_2(y) = 1/2 \max\{L, C_H, C_L\}\|y\|^2$ such that $W_1(y) \leq V(y) \leq W_2(y)$, the uniform stability of $y = 0$ is proved.

Equipped with the above Lemma, it makes sense to assume that all the variables are bounded, and in particular there exist X_1^- and positive scalars $X_1^+, X_2^-, X_2^+, X_3^+$, such that

$$X_1^- \leq x_1 \leq X_1^+, \tag{12}$$

$$X_2^- \leq x_2 \leq X_2^+, \tag{13}$$

$$0 < x_3 \leq X_3^+, \tag{14}$$

Strictly speaking, the hypothesis of positivity of x_2 and x_3 does not come directly from Lemma 1, but is a trivial requirement in this kind of applications, and is physically sound.

Moreover, although the lemma considers the case of time-varying control u, in practical implementations the control always approaches constant values, since stepwise constant references are used. Then it will be useful to denote by $x_u^*(\alpha) = \left[x_{1u}^*(\alpha) \;\; x_{2u}^*(\alpha) \;\; x_{3u}^*(\alpha)\right]^T$ the steady-state solution of the system (1)–(3) with *any* fixed u in the interval [0, 1] and for a given α in (2).[1]

It is of particular interest the investigation of stability of the steady-state solutions in both extreme configurations (namely $u \equiv 0$ and $u \equiv 1$, fixed). It is clear that in both configurations, system (1)–(3) reduces to an LTI system. Specifically, for $u \equiv 0$, the system has a globally exponentially stable equilibrium point at

$$\begin{aligned} x_{10}^* &= -\frac{E_L}{R_L} \\ x_{20}^* &= \frac{R_{DH}}{R_H} E_H \\ x_{30}^* &= 0. \end{aligned} \tag{15}$$

Analogously, when $u \equiv 1$, the dynamic matrix is

$$\begin{bmatrix} 0 & \frac{1}{L} & -\frac{1}{L} \\ -\frac{1}{C_H} & -\alpha & 0 \\ \frac{1}{C_L} & 0 & -\frac{1}{R_L C_L} \end{bmatrix}, \tag{16}$$

that is clearly Hurwitz (it is sufficient to apply the Routh–Hurwitz criterion) and the globally exponentially stable equilibrium point is at

$$\begin{aligned} x_{11}^* &= \frac{R_{DH}/R_H\, E_H - E_L}{R_{DH} + R_L} \\ x_{21}^* &= \frac{R_{DH} R_L}{R_{DH} + R_L}\left(\frac{E_H}{R_H} + \frac{E_L}{R_L}\right) \\ x_{31}^* &= x_{21}^*. \end{aligned} \tag{17}$$

These properties will be used in the next Section.

3.2. Low-level control

The control objectives will be translated on the definition of a time-varying sliding manifold

$$\mathcal{S} = \{(k(t), x) | \sigma(k(t), x) = 0, \forall t \geq 0\} \tag{18}$$

[1] For the sake of notational simplicity we will drop the dependence of the solution on α hereafter.

where the sliding function $\sigma(k(t), x)$ is

$$\sigma(k(t), x) = k(t)x_2 - x_1 \tag{19}$$

and $k(t)$ is a design adaptive parameter. The basic idea is that when $\sigma(k(t), x) = 0$, i.e., the state is on the manifold $\mathcal{S}$, the control objective has been achieved for a suitable value k chosen adaptively. A similar approach to this problem has already been proposed in Cavallo, Canciello, and Guida (2018) through High-Gain Control Theory and Tikhonov's Theorem on the infinite time horizon. We here just recall the final results of Cavallo, Canciello, and Guida (2018) since they will be used later in this paper. The key point is that the parameter $k(t)$ has to be chosen so that it asymptotically approaches the value k_1^*,

$$k_1^* = \frac{E_H - \sqrt{E_H^2 - 4R_H^2 C_H \bar{x}_1 (R_L \bar{x}_1 + E_L)\alpha}}{2R_H(R_L\bar{x}_1 + E_L)} \tag{20}$$

in the case of battery recharging, assuming a constant current recharge, i.e., a constant reference $\bar{x}_1$ for the inductor current. In the case of generator current limitation, $k(t)$ must approach

$$k_2^* = \frac{-E_L + \sqrt{E_L^2 - 4R_L\bar{x}_2(\alpha C_H \bar{x}_2 - E_H/R_H)}}{2R_L\bar{x}_2} \tag{21}$$

where $\bar{x}_2$ is a prescribed voltage reference such that the generator current does not go beyond an upper bound (see later). However, the control strategy proposed above presents several drawbacks. The parameter k in (20) and (21) is chosen assuming that the load value is known, which is not always the case in practical applications. Moreover, the computation of the parameter k is done exploiting the knowledge of most of the system parameters. This may translate into poor robustness of the control algorithm since small variations of the actual value of the system parameters cause an erroneous computation of k, thus a wrong definition of the sliding manifold.

An alternative approach has been proposed in Cavallo, Canciello, Guida et al. (2018), where possible values of the load have been preliminarily identified by using statistic approaches, but the robustness of the approach is still an open issue. It is clear that the preferred solution is the design of an adaptive control law, yielding more robust characteristics and the capability of achieving the control goal even when the system load is not known. In this work, the parameter $k(t)$ is chosen adaptively. In the case of battery charging with constant current $\bar{x}_1$, k is chosen so as to satisfy

$$\dot{k} = \gamma_1(\bar{x}_1 - x_1) \tag{22}$$

with γ_1 being a positive constant to be chosen and $\bar{x}_1$ the current reference to be tracked. It will be shown that a first order Sliding Mode Control is enforced and the control law

$$u = \begin{cases} 0 & \text{when } \sigma \le 0 \\ 1 & \text{when } \sigma > 0 \end{cases} \tag{23}$$

guarantees that the sliding manifold (18) is reached in finite time. Moreover, the closed-loop system converges to an asymptotically stable equilibrium point.

The above considerations are formalised in the following Theorem.

Theorem 2 (*Adaptive Current Control*). *Consider the system (1)–(3) and the control law (23) where the sliding function is defined as in (19) and the parameter k is chosen adaptively according to (22). Assume*

$$x_{3u}^*/x_{2u}^* < 1 \tag{24}$$

$$x_{10}^* < \bar{x}_1 < x_{11}^*, \tag{25}$$

$$X_3^+ < X_2^- \tag{26}$$

and let $|k| < K_{\max}$ *with*

$$K_{\max} < \min\left\{ \frac{X_3^-}{L|\psi_1|}, \frac{X_2^- - X_3^+}{L\left(\frac{|\psi_2|}{C_H} + \psi_3\right)} \right\} \tag{27}$$

and $\psi_1 := \min\left\{\beta_H - \alpha X_2^+, -\left(\beta_H - \alpha X_2^-\right)\right\}$,
$\psi_2 := \min\left\{X_1^-, -X_1^+\right\}$ *and*
$\psi_3 := \max\left\{\beta_H - \alpha X_2^+, -\left(\beta_H - \alpha X_2^-\right)\right\}$.
Then, defining

$$a(\gamma_1) = \gamma_1 L {x_{2u}^*}^3 - \frac{R_L}{4}\frac{{x_{2u}^*}^3}{x_{3u}^*} - \frac{1}{4}\frac{{x_{3u}^*}^2}{\gamma_1 L k_1^* \bar{x}_1} \tag{28}$$

$$b(\gamma_1) = \alpha C_H - 3\gamma_1 L k_1^* \bar{x}_1 \tag{29}$$

choosing $\gamma_1 > 0$ *such that*

$$\gamma_1 < \min\left\{ \frac{X_3^-/L + K_{\max}\psi_1}{\left(X_1^+ - \bar{x}_1\right)X_2^+}, \right.$$
$$\left. \frac{1}{\left(\bar{x}_1 - X_1^-\right)X_2^+}\left[\frac{X_2^- - X_3^+}{L} - K_{\max}\left(\frac{|\psi_2|}{C_H} + \psi_3\right)\right] \right\} \tag{30}$$

and such that

$$\nu = \min\{a(\gamma_1), b(\gamma_1)\} > 0 \tag{31}$$

the closed-loop system has the property that for any $\epsilon > 0$ *there exist* $T > 0$ *such that*

$$|\bar{x}_1 - x_1(t)| < \epsilon \qquad \forall t > T. \tag{32}$$

Moreover, the system state reaches the positively invariant set $\mathcal{S}$ (18) *in finite time.*

Proof. The proof is based on the Theory of Sliding Mode.

First, the reaching and the existence conditions of the sliding mode are shown, then the stability of the zero-dynamics in sliding regime is proven. In order to prove the reaching condition, we need to demonstrate that starting either from $\sigma(k(0), x(0)) < 0$ or from $\sigma(k(0), x(0)) > 0$, the sliding manifold $\sigma(k(t), x) = 0$ is reached in finite time. Let us consider the case $\sigma(k(0), x(0)) < 0$, thus $u \equiv 0$, first. In this case, the system exponentially tends towards $\begin{bmatrix} x_{10}^* & x_{20}^* & x_{30}^* \end{bmatrix}^T$ and, given (22) and (25), k eventually will be increasing. Therefore there must be a time t^* such that the system trajectory crosses the sliding surface. Analogously, for $\sigma(k(0), x(0)) > 0$, the initial control input is $u \equiv 1$. In this case the system exponentially tends towards $\begin{bmatrix} x_{11}^* & x_{21}^* & x_{31}^* \end{bmatrix}^T$ and k eventually decreases with time (note that, due to (5), $x_{11}^* > 0$), hence, also in this case, the system trajectory crosses the sliding surface. The sliding mode existence property is guaranteed by proving

$$\sigma\dot{\sigma} < -\omega|\sigma|, \quad \text{as} \quad \sigma \to 0 \tag{33}$$

with $\omega > 0$. Basically, the proof is based on the computation of $\dot{\sigma}$

$$\begin{aligned} \sigma\dot{\sigma} &= \left(\dot{k}x_2 + k\dot{x}_2 - \dot{x}_1\right)\sigma \\ &= \left[-\frac{1}{2}\left(\frac{kx_1}{C_H} + \frac{x_2}{L}\right) + \dot{k}x_2 + \frac{x_3}{L} + k\left(\beta_H - \alpha x_2\right)\right]\sigma \\ &\quad - \frac{1}{2}\left(\frac{kx_1}{C_H} + \frac{x_2}{L}\right)|\sigma| = (\phi_1 - \phi_2)\,\sigma - \phi_2|\sigma| \end{aligned} \tag{34}$$

with $\phi_1 := \dot{k}x_2 + \frac{x_3}{L} + k\left(\beta_H - \alpha x_2\right)$ and $\phi_2 := \frac{1}{2}\left(\frac{kx_1}{C_H} + \frac{x_2}{L}\right)$. Then it is easy to verify that $\sigma\dot{\sigma} < -\omega|\sigma|$ holds if and only if it holds

$$\begin{cases} \phi_1 > 0, \\ 2\phi_2 - \phi_1 > 0. \end{cases} \tag{35}$$

Let us verify the first condition, namely $\phi_1 > 0$ by taking into account the worst case scenario. It is easy to verify that $\phi_1 > 0$ holds if γ_1 is chosen such that

$$\gamma_1 < \frac{X_3^-/L + K_{\max}\psi_1}{\left(X_1^+ - \bar{x}_1\right)X_2^+}. \tag{36}$$

Note that, in order for γ_1 to be positive it must hold

$$K_{\max} < \frac{X_3^-}{L|\psi_1|}. \tag{37}$$

Similarly, γ_1 can be properly selected in order to obtain $2\phi_2 - \phi_1 > 0$ which holds if

$$\gamma_1 < \frac{1}{(\bar{x}_1 - X_1^-)X_2^+}\left[\frac{X_2^- - X_3^+}{L} - K_{\max}\left(\frac{|\psi_2|}{C_H} + \psi_3\right)\right], \tag{38}$$

where $K_{\max}$ must be chosen such that

$$K_{\max} < \frac{X_2^- - X_3^+}{L\left(\frac{|\psi_2|}{C_H} + \psi_3\right)} \tag{39}$$

in order to guarantee positivity of γ_1. Thus the system trajectory reaches the sliding manifold and remains onto it in finite time. Moreover, in order to consider the tightest estimate of the decay rate of σ, ω can be selected as

$$\omega = \min\{\phi_1, 2\phi_2 - \phi_1\}. \tag{40}$$

Hereafter, stability of the system trajectories constrained on the manifold must be studied. Once on the manifold, the sliding function is identically zero, therefore $\sigma \equiv 0$ and $\dot{\sigma} = 0$. Solving $\dot{\sigma} = 0$ for u with $\sigma \equiv 0$, the equivalent control can be computed

$$u_{eq} = \frac{LC_H}{(Lk^2 + C_H)x_2}\left[\left(\dot{k} - \alpha k\right)x_2 + \frac{x_3}{L} + \beta_H k\right] \tag{41}$$

Replacing (41) in (2) and (3), the equations of the system sliding on the manifold (reduced order system) are obtained

$$\dot{k} = \gamma_1(\bar{x}_1 - kx_2) \tag{42}$$

$$\dot{x}_2 = -\alpha x_2 - \frac{1}{C_H}kx_2u_{eq} + \beta_H \tag{43}$$

$$\dot{x}_3 = \frac{1}{C_L}kx_2 - \frac{1}{R_LC_L}x_3 + \beta_L \tag{44}$$

Stability of the equilibrium point of this system can be studied resorting to Lyapunov theory. Preliminarily, the equilibrium point of the system is translated to the origin by using the new state $z \in \mathbf{R}^3$, with $z_1 = k - k_1^*$, $z_2 = x_2 - x_{2u}^*$ and $z_3 = x_3 - x_{3u}^*$, the superscript $(\cdot)^*$ denoting the steady-state solution. Thus, in the new coordinates one has

$$\dot{z}_1 = -\gamma_1\left[z_1\left(z_2 + x_{2u}^*\right) + k_1^*z_2\right] \tag{45}$$

$$\dot{z}_2 = \frac{1}{L\left(z_1 + k_1^*\right)^2 + C_H}\left[-L\left(z_1 + k_1^*\right)\left(z_2 + x_{2u}^*\right)\dot{z}_1 - \alpha C_H z_2 - z_3\left(z_1 + k_1^*\right) - x_{3u}^*z_1\right] \tag{46}$$

$$\dot{z}_3 = -\frac{1}{R_LC_L}z_3 - \frac{1}{C_L\gamma_1}\dot{z}_1 \tag{47}$$

Let us consider the Lyapunov function

$$V(z) = \frac{Lx_{2u}^{*2}}{2}z_1^2 + \frac{1}{2}z_2^2\left[L\left(z_1 + k_1^*\right)^2 + C_H\right] + \frac{C_L}{2}z_3^2 \tag{48}$$

whose time derivative is

$$\dot{V}(z) = -z^T\begin{bmatrix}\gamma_1 Lx_{2u}^{*3} & 0 & 0\\ 0 & \alpha C_H - \gamma_1 Lk_1^*\bar{x}_1 & 0\\ 0 & 0 & \frac{1}{R_L}\end{bmatrix}z$$

$$+\gamma_1 Lx_{2u}^*z_1z_2^2\left(z_1 + 2k_1^*\right) + z_1\left(x_{2u}^*z_3 - x_{3u}^*z_2\right) \tag{49}$$

After some algebraic manipulation, the following expression is obtained

$$\dot{V}(z) \le -a(\gamma_1)z_1^2 - b(\gamma_1)z_2^2 - cz_3^2 + \frac{1}{2}\gamma_1 Lx_{2u}^*\left(z_1^2 + z_2^2\right)^2 \tag{50}$$

where

$$c = \frac{1}{R_L} - \frac{1}{R_L}\frac{x_{3u}^*}{x_{2u}^*} \tag{51}$$

In the above derivation the well-known inequality $|xy| \le \frac{1}{2}\left(\rho^2x^2 + y^2/\rho^2\right)$ for any $\rho \in \mathbf{R}$ has been extensively used. Note that $c > 0$ due to (24), $a(\gamma_1)$ and $b(\gamma_1)$ impose respectively a lower and an upper bound on the choice of the gain γ_1. Considering hypothesis (31) and denoting $\hat{z} = [z_1 \quad z_2]^T$

$$\begin{aligned}\dot{V}(z) &\le -\nu\|\hat{z}\|^2 + \frac{1}{2}\gamma_1 Lx_{2u}^*\|\hat{z}\|^4 - cz_3^2\\ &= -\|\hat{z}\|^2\left(\nu - \frac{1}{2}\gamma_1 Lx_{2u}^*\|\hat{z}\|^2\right) - cz_3^2\end{aligned} \tag{52}$$

Therefore, (52) will be negative definite in a cylinder of radius $\|\hat{z}\|$ such that

$$\|\hat{z}\| < \sqrt{\frac{2}{\gamma_1 Lx_{2u}^*}\nu} \tag{53}$$

Hence local asymptotic stability of the origin and an estimate of the region of attraction have been proved.

Some remarks are now in order.

Remark 3 (*Feasibility*)**.** Condition (24) simply says that there are well-defined LV and HV voltage side, in the sense that it is not possible that in some working condition HV becomes smaller then LV. Condition (26) better quantifies this voltage relationship between LV and HV side. Condition (25) is obvious in practical applications, simply the current cannot exceed the values it has in the extreme cases ($u = 0$ or $u = 1$). Condition $|k| < K_{\max}$ can be easily ensured by using a saturated integral to compute k from (22). Finally, conditions (24)–(26) ensure that (35) hold, hence the existence of the sliding mode.

The second task of the control is to limit the generator current, and this is enforced by considering a reference value $\bar{x}_2$ that the HV capacitor voltage has to track (see also Remark 7). Also in this case we consider the sliding manifold (18), with sliding function (19). However, now the adaptation strategy changes as follows

$$\dot{k} = \gamma_2(x_2 - \bar{x}_2) \tag{54}$$

with $\gamma_2 > 0$. Note that the reference voltage has to be selected so that

$$0 < \bar{x}_2 < \frac{1}{2}\frac{R_{DH}}{R_H}E_H\left[1 + \sqrt{1 + \frac{R_H}{R_{DH}}\frac{C_H}{C_L}\left(\frac{E_L}{E_H}\right)^2}\right] \tag{55}$$

where the upper bound comes from Corollary 2 in Cavallo, Canciello, and Guida (2018). Also in this case, the control law (23) guarantees that the sliding manifold (18) is reached in finite time, as it will be shown below. Stability of the adaptive law in the case of voltage control is considerably harder to show than in the case of current tracking. Preliminarily, define the following symbols

$$\Delta E = \sqrt{E_L^2 - 4\bar{x}_2\frac{R_L}{R_H}\left[\left(1 + \frac{R_H}{R_D}\right)\bar{x}_2 - E_H\right]} - E_L \tag{56}$$

$$\hat{\gamma}_2 = \frac{2}{L}\frac{C_H}{C_L}\frac{1+\left(1+\frac{R_H}{R_D}\right)\frac{R_L}{R_H}\frac{C_L}{C_H}}{\Delta E} + \frac{\Delta E}{2C_L R_L^2 \bar{x}_2^2} \tag{57}$$

$$a_0 = \frac{1}{2}(\Delta E + E_L) \tag{58}$$

$$a_{10} = \frac{1}{\bar{x}_2}\left(\frac{E_H}{R_H} - \frac{E_L}{R_L}\frac{\Delta E - E_L}{2\bar{x}_2}\right) \tag{59}$$

$$a_{11} = \left[\frac{L}{R_L}(\Delta E - E_L) + R_L C_L(\Delta E + E_L)\right] \tag{60}$$

$$a_{20} = \frac{1}{2}LC_L\hat{\gamma}_2(\Delta E - E_L) \tag{61}$$

$$a_{21} = \frac{1}{2}LC_L(\Delta E - E_L) \tag{62}$$

$$a_3 = (R_L C_L)^2\left[\frac{1}{2}\frac{L}{R_L}\hat{\gamma}_2(\Delta E - E_L) - \frac{R_D + R_H}{R_D R_H}\right] \tag{63}$$

Finally, define the polynomial equation

$$p(\gamma) = a_{11}a_{21}\gamma^2 + (a_{11}a_{20} + a_{10}a_{21} - a_3 a_0)\gamma + a_{10}a_{20} = 0 \tag{64}$$

and let γ^+ be the smallest *real positive* solution (if any) of (64). If (64) has only complex or real negative solutions, we let $\gamma^+ = \infty$. Now we are in the position to state the following Theorem.

Theorem 4 (*Adaptive Voltage Control*)**.** *Consider the system (1)–(3) and the control law (23) where the sliding function is defined as in (19) and the parameter k is chosen adaptively according to (54). Suppose*

$$R_D > \frac{\bar{x}_2}{E_H - \bar{x}_2}R_H \tag{65}$$

Then γ_2 can be any positive scalar. If otherwise

$$R_D \le \frac{\bar{x}_2}{E_H - \bar{x}_2}R_H \tag{66}$$

then select $\gamma_2 < \min(\hat{\gamma}_2, \gamma^+)$. Assume

$$x_{21}^* < \bar{x}_2 < x_{20}^*, \tag{67}$$

$$X_3^+ < X_2^- \tag{68}$$

and let $|k| < K_{\max}$ with $K_{\max}$ as in (27) and ψ_1, ψ_2 and ψ_3 selected as in Theorem 2. Then, choosing $\gamma_2 > 0$ such that the additional condition

$$\gamma_2 < \min\left\{\frac{X_3^-/L + K_{\max}\psi_1}{(X_2^+ - \bar{x}_2)X_2^+}, \frac{1}{(X_2^+ - \bar{x}_2)X_2^+}\left[\frac{X_2^- - X_3^+}{L} - K_{\max}\left(\frac{|\psi_2|}{C_H} + \psi_3\right)\right]\right\}, \tag{69}$$

is satisfied, the closed-loop system converges locally asymptotically to a unique steady-state solution with $x_{2u}^* = \bar{x}_2$, and for any $\delta > 0$ there exists a $T > 0$ such that

$$|\bar{x}_2 - x_2(t)| < \delta \qquad \forall t > T \tag{70}$$

Moreover, the system state reaches the positively invariant set $\mathcal{S}$ (18) in finite time.

Proof. As in the proof of Theorem 2, we have to prove that the sliding manifold is reached first, and then the stability of the system on the manifold. The proof of reaching follows the same steps as in Theorem 2, with the due modification of the upper bound on γ_2, and is omitted for the sake of brevity. Once the sliding has been established, The stability on the manifold has to be proved. The equivalent control is again (41), but (42) changes to (54). Consider the coordinate translation

$$z_1 = k - k_2^* \tag{71}$$

$$z_2 = x_2 - \bar{x}_2 \tag{72}$$

$$z_3 = x_3 - x_{3u}^* \tag{73}$$

Then the dynamic of the translated system is given by

$$\dot{z}_1 = \gamma_2 z_2 \tag{74}$$

$$\dot{z}_2 = \frac{1}{L(z_1 + k_2^*)^2 + C_H}\left[-L(z_1 + k_2^*)(z_2 + \bar{x}_2)\gamma_2 z_2 - \alpha C_H z_2 - z_3(z_1 + k_2^*) - x_{3u}^* z_1\right] \tag{75}$$

$$\dot{z}_3 = -\frac{1}{R_L C_L}z_3 + \frac{1}{C_L}(z_1 z_2 + k_2^* z_2 + \bar{x}_2 z_1) \tag{76}$$

Local stability of the origin of the system (74)–(76) can be assessed locally by linearisation. The dynamic matrix can be computed as

$$A = \begin{bmatrix} 0 & \gamma_2 & 0 \\ -\frac{x_{3u}^*}{Lk_2^{*2}+C_H} & -\frac{\alpha C_H + \gamma_2 L k_2^* \bar{x}_2}{Lk_2^{*2}+C_H} & -\frac{k_2^*}{Lk_2^{*2}+C_H} \\ \frac{\bar{x}_2}{C_L} & \frac{k_2^*}{C_L} & -\frac{1}{R_L C_L} \end{bmatrix} \tag{77}$$

whose characteristic polynomial is

$$\begin{aligned} q(s) &= s\left(s^2 + \frac{Lk_2^{*2} + C_H + \alpha C_H R_L C_L}{R_L C_L(Lk_2^{*2} + C_H)}s + \frac{R_L k_2^{*2} + \alpha C_H}{R_L C_L(Lk_2^{*2} + C_H)}\right) + \gamma_2\left(\frac{Lk_2^*\bar{x}_2}{Lk_2^{*2} + C_H}s^2 + \frac{R_L C_L x_{3u}^* + Lk_2^*\bar{x}_2}{Lk_2^{*2} + C_H}s + \frac{R_L k_2^*\bar{x}_2 + x_{3u}^*}{Lk_2^{*2} + C_H}\right) \\ &\triangleq a(s) + \gamma_2 b(s) \end{aligned} \tag{78}$$

Stability of system (74)–(76) for different values of γ_2 can be analysed by using root locus analysis. Note that, although $\bar{x}_2 > 0$, the sign of k_2^* is not known *apriori*. However, if (65) holds, it is possible to show, by algebraic calculation, that $k_2^* > 0$. In this case both the polynomials $a(s)$ and $b(s)$ in (78) have roots in the closed complex left half-plane, and the stability is assured by any $\gamma_2 > 0$. On the contrary, if (66) holds, k_2^* is surely negative. In this case the stability holds for $\gamma_2 > 0$ only if $2R_L k_2^* \bar{x}_2 + E_L$ is imposed positive. In this case the polynomial $b(s)$ has one positive and one negative root, hence there will be an upper bound to the stabilising values of γ_2. The upper bound can be sought by using Routh–Hurwitz criterion. After some algebraic computation, the following stability conditions must be satisfied.

$$\gamma_2 < \hat{\gamma}_2 \tag{79}$$

and, if the polynomial $p(\lambda_2)$ has real roots, denote them by γ_2' and γ_2'', with $\gamma_2' < \gamma_2''$,

$$\gamma_2 < \gamma_2'' \text{ if } a_{11}a_{21} < 0 \tag{80}$$

$$\gamma_2 < \gamma_2' \text{ or } \gamma_2 > \gamma_2'' \text{ otherwise} \tag{81}$$

note that if $a_{11}a_{21} < 0$, then $\gamma_2' < 0$. The above conditions are implied by $\gamma_2 < \min(\hat{\gamma}_2, \gamma^+)$. This concludes the proof.

Remark 5 (*Adaptation Gain*)**.** From the proof of Theorem 4 it can be shown that if the load satisfies (66), then a *negative* γ_2 could be sought to stabilise the closed-loop system. However, in practical applications often the load is unknown, and since negative γ_2 are destabilising for the case (65), the solution is to use the smallest *positive* γ_2 stabilising any load.

Remark 6 (*Reaching Time*)**.** It is easy to estimate the reaching time (Slotine & Li, 1991, Chap. 7) for the case of battery current regulation

$$t_{reach} \leq \sigma(0)/\omega \tag{82}$$

with ω given in (40). With the same approach, a similar estimate holds also for the control strategy presented in Theorem 4. Details are omitted.

Remark 7 (*Robust Implementation*)**.** The choice of the adaptation law (54) is based on the algebraic relationship $x_2 = E_H - R_H I_g$ so that, the generator current can be limited to a prescribed overload current I_{OL} by considering a reference voltage

$$\bar{x}_2 = E_H - R_H I_{OL}. \tag{83}$$

However, the estimate of $\bar{x}_2$ is prone to errors due to possible uncertainties in R_H and E_H. Hence, assuming the generator current measurement available, a better and more robust adaptive law is simply

$$\dot{k} = \gamma_2'(I_{OL} - I_g) \tag{84}$$

where $\gamma_2' = R_H \gamma_2$ is a positive gain.

Remark 8 (*ROA Estimate*)**.** From the above derivation, it is clear that obtaining an analytic estimate of the Region of Attraction (ROA) is considerably harder in the case of voltage control, Theorem 4, than in the case of Theorem 2. However, a numeric estimate of the ROA is possible by using a techniques proposed in Chesi (2011) and starting from a Lyapunov function computed for the linearised case. In particular, since we are interested in reaching the steady-state within 5s, for a given load R_D and reference voltage $\bar{x}_2$, considering the model (74)–(76) compute the dynamic matrix A (77) such that the related Lyapunov function $V = x^T P x$ has decay rate less than 0.75 (so that after about 3s the transient can be considered vanished). This can be accomplished by solving the Lyapunov equation

$$(A^T + 0.75 I_3)P + P(A + 0.75 I_3) = -I_3 \tag{85}$$

for a positive solution P, being I_3 the identity matrix in $\mathbb{R}^{3\times 3}$. Then define the Lyapunov function $V(z) = z^T P z$, with $z = [z_1, z_2, z_3]^T$. Note that, being $V(z)$ quadratic, its derivative along the trajectory of (74)–(76), $\dot{V} = \Delta V \dot{z}$ is a fractional function, since the gradient ΔV is linear in z and the entries of $\dot{z}$ are ratios of polynomial in z. Thus, it is easy to show that $\dot{V}$ is the ratio of a rather complex polynomial numerator, call it $N(z)$ and the *positive* polynomial $L(z_1 + k_2^*)^2 + C_H$. Thus, the problem of computing an estimate of the ROA can be reduced to solving a sequence of Semidefinite Programs (Chesi, 2011, Chapter 2.2). Note that in general the positive solution of (85) is not guaranteed to exist. Another possibility is to start from the Lyapunov function *maximising* the decay rate of the closed-loop system (Boyd, El Ghaoui, Feron, & Balakrishnan, 1994), obtained by solving the Generalised Eigenvalue Problem (GEVP)

$$\begin{aligned} &\max \lambda \\ &\text{subject to } \; P > 0, \quad A^T P + PA + 2\lambda P \leq 0 \end{aligned} \tag{86}$$

and then again using the procedure in Chesi (2011) for the estimate of the ROA. The effectiveness of this approach will be illustrated in Section 4.

Remark 9. The proposed adaptive version of the linearising algorithm in Cavallo, Canciello, and Guida (2018) not only solves the problem of estimating the unknown load R_D, but also is robust to uncertainties in the parameters of the system (busses, energy sources, electric components of the converter), thus simultaneously solving the mismatch between nominal and actual system parameters that in Cavallo, Canciello, Guida et al. (2018) was faced by using classification approaches.

3.3. High-level control

In view of what has been expressed above, it is clear that the entire BBCU has at least two main operational modalities: charging the battery, when the generator can accomplish the objective of feeding the grid loads keeping its current below a prescribed threshold, and regulating the generator current to a prescribed level in order to let the battery help the generator when an overload occurs. This can be accomplished with a simple automaton using just two modes. Specifically

- Mode 1: the generator on the high voltage side recharges the battery with a constant current $\bar{x}_1$ choosing the adaptive parameter $k(t)$ as in (22).
- Mode 2: if an overload occurs the supervisor must commute to Mode 2 to regulate the generator current (equivalently, the high voltage capacitor voltage) to a prescribed current set-point I_{OL} (equivalently, $\bar{x}_2$), possibly asking the battery to provide energy to loads. In this case, the adaptive parameter $k(t)$ is chosen as in (84).

Moreover, for ensuring a safe commutation between the two modes, an estimate of the region of attraction is computed in both operational modes. The overall strategy works as follows. Initially the system is in Mode 1 (assumed in the region of attraction of the controller). Next, if an overload occurs, Mode 2 is activated. However, before entering Mode 2 we must be sure that, after the finite time needed to reach the new sliding manifold, the system state belongs to the region of attraction of the new active controller configuration, i.e., Mode 2. This is done comparing the current state and the estimate of the region of attraction for the new controller configuration. If the state is in the interior of the region of attraction, then the transition to Mode 2 is enabled, otherwise, a reduced performance mode is activated, with I_{OL} increased so that the current state is within the reduced-performance ROA. This point will be clarified in Section 4.2. Next, the generator current is reduced, by slowly reducing the I_{OL} until the original performance are achieved. As soon as the overload ends, the generator is still supplying I_{OL}, thus there is an excess of current that flows in the inductor. By detecting this extra-current the supervisor decides the transition back to Mode 1. This is different from the approach in Cavallo et al. (2017).

4. Numerical estimate of the ROA and simulation results

The proposed adaptive sliding control and associated supervisory strategy for MEA have been tested in a detailed MATLAB/Simulink/SimPowerSystem simulator, shown in Fig. 2, and composed of five blocks:

- LOAD: contains a bank of parallel resistors (yellow block).
- SUPERVISOR: implements the High-Level Control designed according to Section 3.3 (green block).
- ADAPTIVE LEVEL: estimates the parameter k according to (22) and (54) (orange block).
- LOW LEVEL CONTROL: implements the Low-Level Control logic according to Section 3.2 (light blue block).
- SWITCHING LOGIC: realises the switching logic for Q_1 and Q_2 switches (red block).

The supervisor is a two-modes automaton, as shown in Fig. 3, and it is been implemented using the MATLAB StateFlow toolbox. It must be noted that, the commutation between states uses tolerance thresholds η_1 and η_{gen} on the inductor and generator currents, respectively. Moreover, the usage of a piecewise constant overload reference is considered in Mode 2 in the supervisor. This will be clarified in Section 4.2.

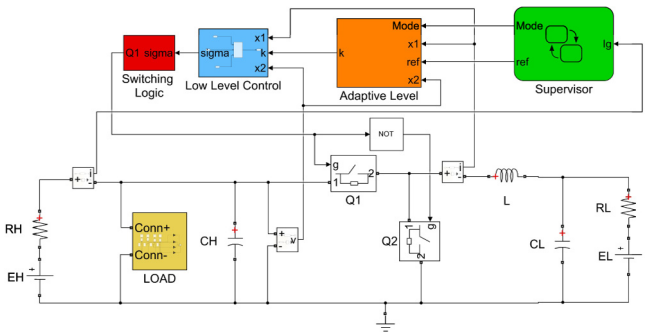

Fig. 2. Simulink scheme of controlled system.

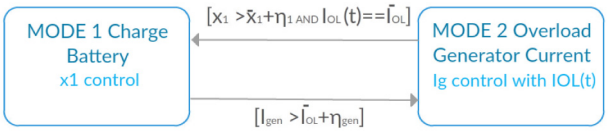

Fig. 3. Supervisor.

Table 1
Simulation parameters.

(a) System parameters		
Parameter	Value	
E_H	270	[V]
R_H	100	[mΩ]
L	10	[mH]
C_H	0.8	[mF]
E_L	28	[V]
R_L	100	[mΩ]
C_L	0.4	[mF]
(b) Controller parameters		
Parameter	Value	
γ_1	4	$[\text{V}\cdot\text{s}]^{-1}$
γ_2	4	$[\text{V}\cdot\Omega\cdot\text{s}]^{-1}$
$\bar{x}_1$	10	[A]
$\bar{I}_{OL}$	16	[A]
η_1	0.5	[A]
η_{gen}	0.5	[A]

The system and controller parameters are shown in Tables 1a–b. The reaching time is estimated according to (82) for the inductor current control, and is 0.14s. A similar computation for the generator current control gives an estimate of the reaching time for the second sliding surface of 0.02s, that will be neglected in the following discussion, due to its small value. Two scenarios have been simulated, as presented in the following sections.

4.1. Scenario 1: small load variations

A preliminary set of simulations has been carried out by considering a stepwise constant load R_D varying from 300Ω to 15Ω. Since, as shown by (20), (21), for low values of R_D the parameter k varies widely, then nonuniform variation of R_D has been considered. Specifically, in the interval $[20, 300]\Omega$ a large step of 70Ω has been selected, in $[17, 20]\Omega$ interval the step has been reduced to 1Ω. Finally, the interval $[15, 17]\Omega$ has been swept with step interval 0.5Ω. The varying load is shown in Fig. 4, with a zoom around the zone with smaller variation of R_D.

The purpose of this first set of simulations is to gain insight in the variation of the gains k associated to the loads and an estimate of the ROA's for the controlled plant with a reasonable set of loads. In this first set of simulations the overload current is fixed

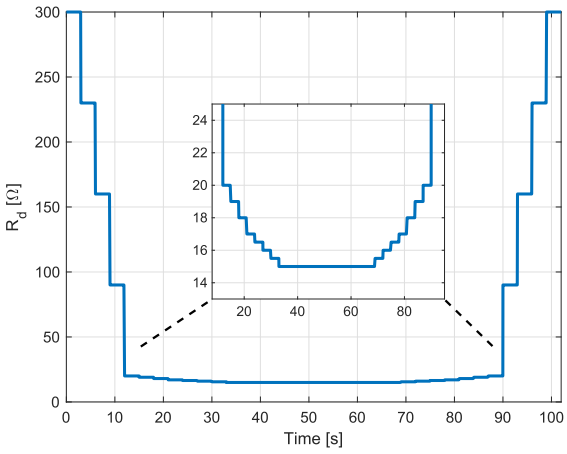

Fig. 4. Load variation in Scenario 1.

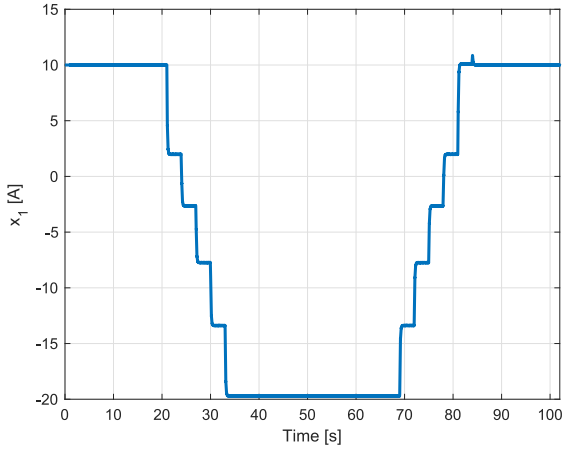

Fig. 5. Inductor current, Scenario 1.

to a constant $\bar{I}_{OL} = 16$A. The simulations starts with $R_D = 300\Omega$. The generator current is below the prescribed threshold ($\bar{I}_{OL}$), therefore no overload occurs. The supervisor is initially in Mode 1, hence the objective is to recharge the battery with constant current ($\bar{x}_1$) through the inductor, as shown in Fig. 5 (first 21s).

Every 3s the load resistor is decreased, and the supervisor for the first 18s remains in Mode 1, with generator current increasing (Fig. 6), but without reaching the threshold of maximum current. At time $t = 18$s, the load becomes $R_D = 18\Omega$ and the current request to the generator becomes $I_g = 16.4$A. Note that, although the requested current exceeds $\bar{I}_{OL}$, the value $\bar{I}_{OL} + \eta_{gen}$ is *not* exceeded, hence the supervisor remains in Mode 1. After 3 more seconds, at $t = 21$s, the load $R_D = 17\Omega$ makes the generator current exceed $\bar{I}_{OL} + \eta_{gen}$, hence the supervisor switches to Mode 2, changing the control objective to drive the generator current to the current threshold $\bar{I}_{OL}$.

In order to guarantee the stability, some considerations on the ROA's are in order. When in Mode 1, the ROA is the cylinder with radius (53). Using the numerical values above and Theorem 2, we have a rough estimate of the ROA is $\|\hat{z}\| < 4.3$, that is a large region in our case. Thus, in this case study, we can safely assume that any load variation in Mode 1 happens when the controlled state is *within* the ROA.

The situation is different when in Mode 2, where, moreover, larger variations of the variables happen. In Fig. 7 the ROA's are shown for different loads. Although the ROA is a 3D region, only its projection on the (x_3, k) plane will be presented, for the sake of

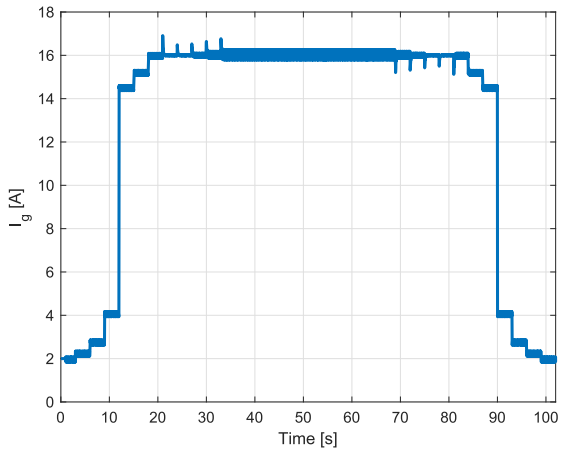

Fig. 6. Generator current, Scenario 1.

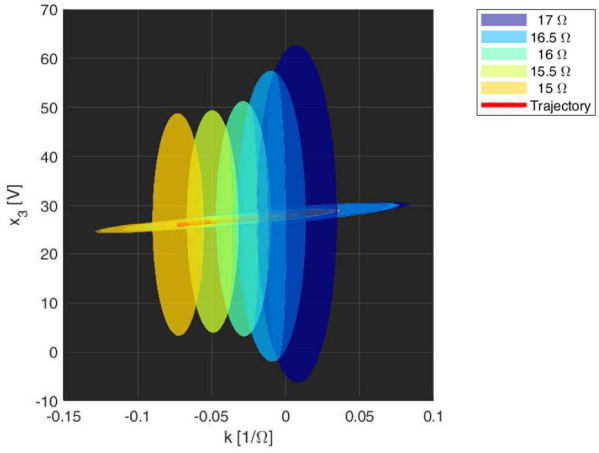

Fig. 7. Variation of the Domain of Attraction as the load varies smoothly.

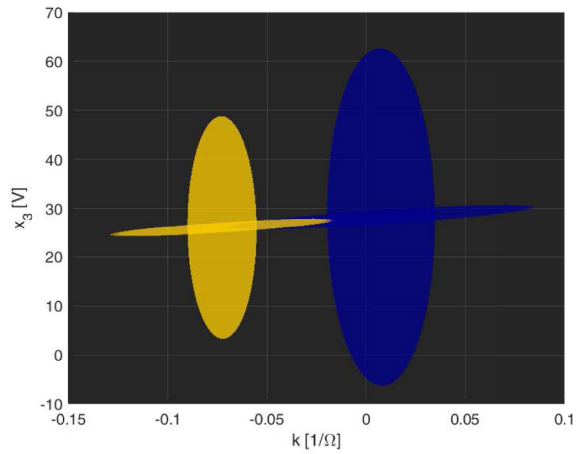

Fig. 8. Variation of the Domain of Attraction as the load varies abruptly. Blue: $R_D = 17\Omega$; yellow: $R_D = 15\Omega$.

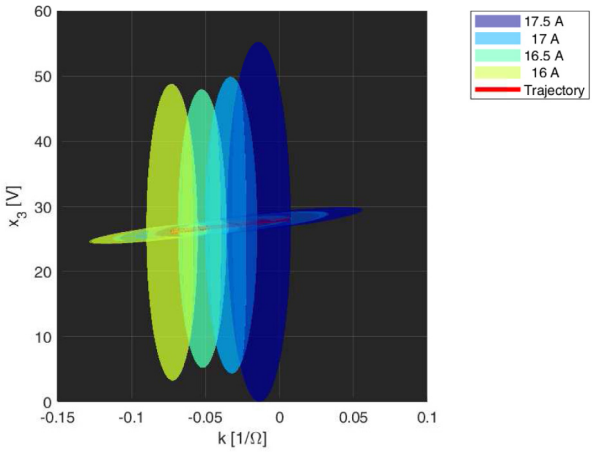

Fig. 9. Variation of the Domain of Attraction as I_{OL} varies with $R_D = 15\Omega$.

clearness. Two estimates of the ROA are computed for each load: one resulting from (85) (thick region) and one from (86) (thin region). The union of the two regions is in the ROA. Note that at $t = 21$s, when the supervisor decides the commutation from Mode 1 to Mode 2, the large blue ROA, that is the ROA of the new control action, includes the current state, hence the supervisor can safely switch to the strategy in Theorem 4. The remaining load variations cause related changes in the steady-state of the closed-loop system. Fig. 7 shows that if the change of load is small and slow enough, stability is preserved. Indeed, for the values of R_D shown in Fig. 7, note that the centre of the ROA associated to a given load belongs to the interior of the ROA associated to the next load (assuming the sequence of loads defined by the load profile in Fig. 4): e.g., the centre of the blue region is within the elongated azure region pertaining to $R_D = 16.5\Omega$, and the centre of the azure region is within the elongated region of the cyan region related to $R_D = 16\Omega$. This shows that a smooth and "slow" transition from $R_D = 17\Omega$ to $R_D = 16\Omega$ preserves stability. Note that "slowness" is related to the optimal decay rate computed by means of (86), hence it can be precisely estimated. In Fig. 7 also the actual trajectory of the system (in red) is shown. Note that, since the ROA's are positively invariant sets, no trajectory exits its ROA.

After 50s the load starts increasing, and after 80s the load is so high that it causes no longer generator overload. As stated at the end of Section 3.3, this is detected by the sudden increase in the inductor current shown in Fig. 5, causing the supervisor to restore Mode 1.

4.2. Large loads variations

Different is the case where there is an abrupt change of load. For instance, in Fig. 8 it is clear that, since the centre of the blue region does not intersect the yellow region, there is no guarantee that the transition from $R_D = 17\Omega$ to $R_D = 15\Omega$ will preserve stability.

A possible solution to this issue is adopt a "transient reduced performance" approach, i.e., to temporarily relax the constraints. If we increase the overload reference current, we have that, with the same R_D, the steady-state of k increases (since less current is needed from the battery) and this observation can be applied to move the leftmost region in Fig. 8 to the right.

To gain insight in the above consideration, we fix the load to $R_D = 15\Omega$ and compute the estimate of the ROA by considering different overload current assuming values in the interval [16, 17.5]A and varying with steps of 0.5A. The result is depicted in Fig. 9, that suggests us how to guarantee stability when the load changes abruptly. Simply, when the load goes to $R_D = 15\Omega$, imposing $I_{OL} = 17.5$A makes the ROA include the centre of the ROA with $R_D = 17\Omega$, $I_{OL} = 16$A, thus preserving stability. Next, by changing the reference smoothly to I_{OL} the original performance are restored with assured stability.

A final consideration is in order. The selection of a reduced performance overload current depends on the knowledge of an estimate of the load. In practical applications sometimes even a

Table 2
Load variation.

Parameter	Resistance [Ω]	Activation time [s]
R_{D1}	300	[0–5] [20–25]
R_{D2}	200	[5–10]
R_{D3}	17	[10–15]
R_{D4}	15	[15–20]

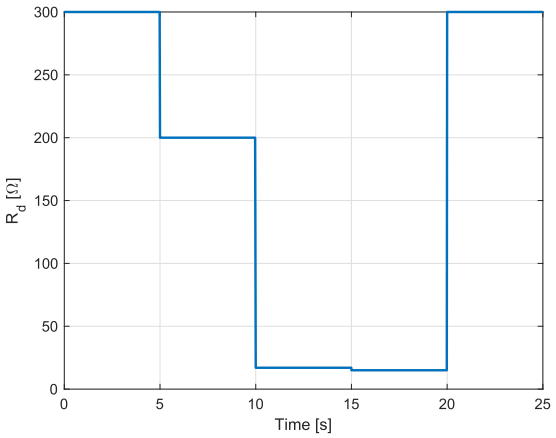

Fig. 10. Load variation in Scenario 2.

rough estimate of the load is not available. In this case a viable strategy is to assume the worst-case scenario, i.e., large variations of the load, and use the "transient reduced performance" approach.

4.3. Scenario 2

The second set of simulations has been carried out referring to the large and unknown load variations in Table 2 and Fig. 10

The supervisor is capable of managing the large load variations described in Section 4.2 as follows. First, the generator current reference decreases from the value 17.5A to $\bar{I}_{OL} = 16A$ in a piece-wise constant fashion in order to guarantee stability. Note that, transition from Mode 2 to Mode 1 is allowed only when the generator reference current has reached the value $\bar{I}_{OL}$. The reference is varied after it has approximately reached its steady-state. The time required for this is estimated based on the worst case of decay time estimated when solving the GEVP (86). Using the above numerical values, one can assess that in the worst case, at least 0.79s are required to reach the steady state with 90% accuracy.

At the beginning of the simulation, the supervisor is in Mode 1 with load $R_D = R_{D1} = 300\Omega$ so the low-level goal is to control the inductor current x_1 to $\bar{x}_1 = 10$A as shown in Fig. 11. Five seconds later a new load is added, and R_D becomes R_{D2}. In this step the generator current increases (Fig. 12), but it is again below the threshold of maximum current hence the supervisor remains in Mode 1. As stated in Section 4.1, load variations always leave the state of the controlled system in the ROA of the current objective, thus stability in Mode 1 is ensured. At time $t = 10$s an additional load is inserted, producing a power request exceeding overload. The supervisor reacts by switching to Mode 2, i.e., changing the control objective to drive the generator current. However, in this case the amplitude of the load variation is unknown, hence, the generator reference is increased to 17.5A in order to guarantee the system stability, as discussed in Section 4.2. Every 0.79s I_{OL} is decreased by 0.5A, until it reaches the threshold $\bar{I}_{OL}$. The result is that the current supplied to the battery is reduced, thus compensating for the increased power demand. At time instant

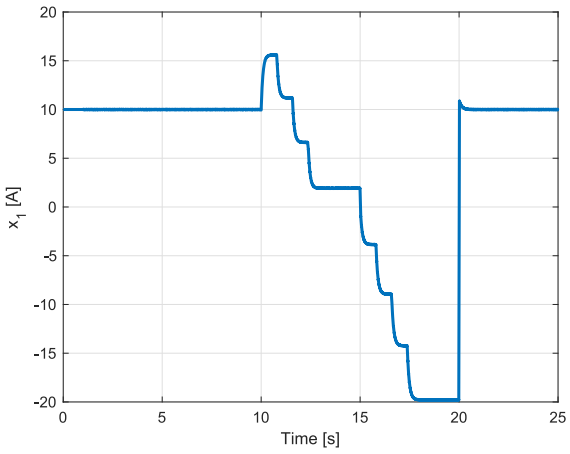

Fig. 11. Inductor current, Scenario 2.

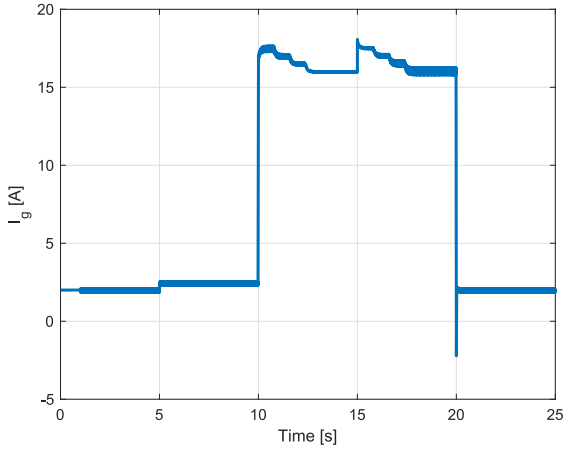

Fig. 12. Generator current, Scenario 2.

$t = 15$s the power request is further increased by reducing the load resistor to $R_D = 15\Omega$. Again, a reduced performance phase starts with $I_{OL} = 17.5$A until the nominal condition $\bar{I}_{OL}$ is restored within 5s. Note that at the end of this phase the inductor current has reversed, so that actually the battery is helping the generator. In Fig. 9 the controlled state trajectory is represented in red. It is always within the ROA's.

Fig. 11 shows the time evolution of the inductor current, and one can note that the proposed controller tracks accurately the current references.

Moreover, in Fig. 12 the generated current is reported. Note that the 5s-capability to suppress the overload is fulfilled.

Fig. 13 shows the time evolution of the parameter k. Finally, Figs. 14 and 15 show the HV and LV voltage, respectively.

5. Conclusions

In this paper the design of a controller for the DC/DC bidirectional converter has been discussed. The future aircraft will depend more and more on electric devices, that must be autonomously operated. A DC/DC converter then is essential device in autonomous management of the loads and energy storage devices (batteries, supercapacitors). The converter has to be controlled, and the control actions can be selected to fulfil different objectives, e.g., to recharge the battery or to use the battery to help the generator in supplying extra-power when requested to do so. A sensible approach is to consider two control layers,

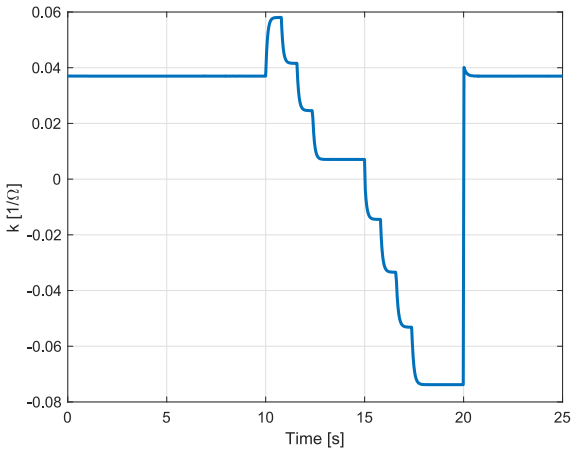

Fig. 13. Adaptive parameter, Scenario 2.

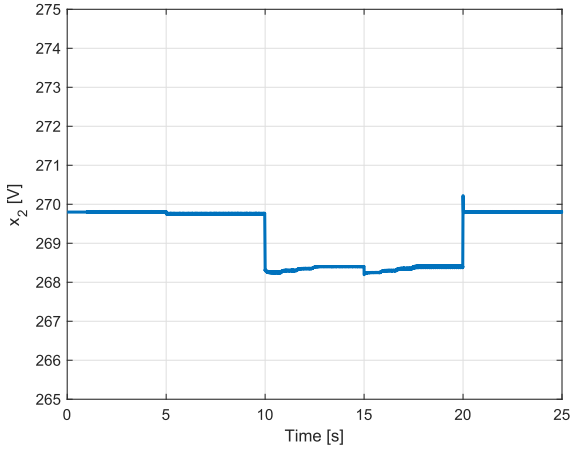

Fig. 14. Capacitor C_H voltage, Scenario 2.

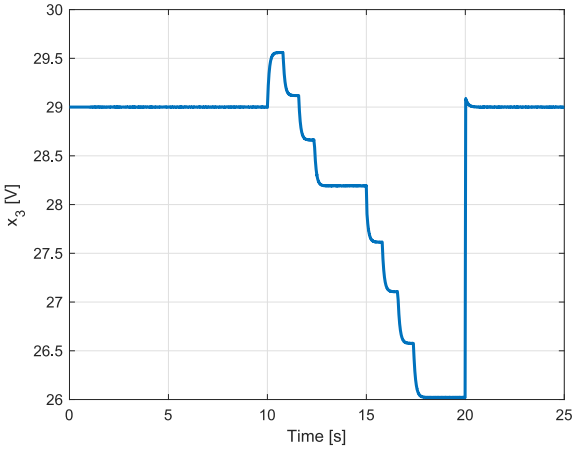

Fig. 15. Capacitor C_L voltage, Scenario 2.

one implementing tracking and/or regulation of some variables with assured stability characteristics, the other coordinating the actions of the low-level controllers. The low-level layer employs an innovative time-varying, adaptive sliding manifold, while a novel high-level supervisor exploits the characterisation of the Regions of Attractions of the low-level controllers to ensure that switching among different control modes can happen only when the state of the controlled system is within the ROA of the next control strategy. Thus, safe switching is ensured. Sometimes, in order to guarantee such a requirement, it can be necessary to consider a transient situation of reduced performances. All the above characteristics are discussed in details in the paper and two different scenarios are considered in a detailed simulation environment considering also switching power electronic devices, showing the effectiveness of the proposed approach.

Acknowledgement

The authors gratefully acknowledge the contribution of Prof. Graziano Chesi for sending us the last version of the software toolbox SMRSOFT.

References

Aeroval Inc. (2020). More electric aircraft (MEA). URL http://www.moreelectricaircraft.com.

Bartolini, G., Ferrara, A., & Usai, E. (1997). Output tracking control of uncertain nonlinear second-order systems. *Automatica*, *33*(12), 2203–2212.

Bartolini, G., Ferrara, A., Utkin, V., & Zolezzi, T. (1997). A control vector simplex approach to variable structure control of nonlinear systems. *International Journal of Robust and Nonlinear Control*, *7*(4), 321–335.

Biel, D., & Fossas, E. (2004). SMC applications in power electronics. In A. Sabanovic., L. Fridman, & S. Spurgeon (Eds.), *Variable structure systems: From principles to implementation* (pp. 265–293). London, UK: The Institution of Electrical Engineers IEE.

Boyd, S., El Ghaoui, L., Feron, E., & Balakrishnan, V. (1994). *Studies in applied mathematics*: *Vol. 15*, *Linear matrix inequalities in system and control theory*. Philadelphia, PA: SIAM.

Branicky, M. S. (1998). Multiple Lyapunov functions and other analysis tools for switched and hybrid systems. *IEEE Transactions on Automatic Control*, *43*(4), 475–482.

Cavallo, A., Canciello, G., & Guida, B. (2017). Supervised control of buck-boost converters for aeronautical applications. *Automatica*, *83*, 73–80.

Cavallo, A., Canciello, G., & Guida, B. (2018). Supervisory control of DC-DC bidirectional converter for advanced aeronautic applications. *International Journal of Robust and Nonlinear Control*, *28*(1), 1–15, rnc.3851.

Cavallo, A., Canciello, G., Guida, B., Kulsangcharoen, P., Yeoh, S., Rashed, M., et al. (2018). Multi-objective supervisory control for DC/DC converters in advanced aeronautic applications. *Energies*, *11*(11).

Cavallo, A., Canciello, G., & Russo, A. (2018). Buck-boost converter control for constant power loads in aeronautical applications. In *2018 IEEE conference on decision and control (CDC)* (pp. 6741–6747).

Cavallo, A., Canciello, G., & Russo, A. (2018). Supervised energy management in advanced aircraft applications. In *2018 European control conference (ECC)* (pp. 2769–2774).

Cavallo, A., Guida, B., Buonanno, A., & Sparaco, E. (2015). Smart buck-boost converter unit operations for aeronautical applications. In *54th IEEE conf. decision control (CDC)* (pp. 4734–4739). http://dx.doi.org/10.1109/CDC.2015.7402957.

Cavallo, A., Russo, A., & Canciello, G. (2019). Control of supercapacitors for smooth EMA operations in aeronautical applications. In *2019 American control conference (ACC)* (pp. 4948–4954).

Cavallo, A., Russo, A., & Canciello, G. (2019). Hierarchical control for generator and battery in the more electric aircraft. *Science China. Information Sciences*, *62*(9), 192207.

Chesi, G. (2011). *Domain of attraction: analysis and control via SOS programming*, *Vol. 415*. London: Springer Science Business Media.

Cucuzzella, M., Rosti, S., Cavallo, A., & Ferrara, A. (2017). Decentralized sliding mode voltage control in DC microgrids. In *Proc. American control conf.*

Durmaz, B., Özgören, M. K., & Salamci, M. U. (2012). Sliding mode control for non-linear systems with adaptive sliding surfaces. *Transactions of the Institute of Measurement and Control*, *34*(1), 56–90.

Fu, J., Zhao, J., & Dimirovski, G. (2006). Robust control of SVC: A new adaptive backstepping method. *Zhongguo Dianji Gongcheng Xuebao/Proceedings of the Chinese Society of Electrical Engineering*, *26*, 7–11.

Hušek, P. (2016). Adaptive sliding mode control with moving sliding surface. *Applied Soft Computing*, *42*.

Incremona, G., Cucuzzella, M., & Ferrara, A. (2016). Adaptive suboptimal second order sliding mode control for microgrids. *International Journal of Control*, *89*, 1849–1867.

Khalil, H. (2002). *Nonlinear systems* (3rd ed.). Prentice Hall.

Levant, A. (1998). Robust exact differentiation via sliding mode technique. *Automatica*, *34*(3), 379–384.

Levant, A. (2003). High-order sliding modes, differentiation and output feedback control. *International Journal of Control*, *76*, 924–941.
Li, L., Zhao, J., & Dimirovski, G. M. (2011). Observer-based reliable exponential stabilization and H_∞ control for switched systems with faulty actuators: An average dwell time approach. *Nonlinear Analysis. Hybrid Systems*, *5*(3), 479–491.
Lopez, O., Garcia De Vicuna, L., Castilla, M., Matas, J., & Lopez, M. (1999). Sliding-mode-control design of a high-power-factor buck-boost rectifier. *IEEE Transactions on Industrial Electronics*, *46*(3), 604–612.
Plestan, F., Shtessel, Y., Brégeault, V., & Poznyak, A. (2010). New methodologies for adaptive sliding mode control. *International Journal of Control*, *83*(9), 1907–1919.
Russo, A., & Cavallo, A. (2020). Supercapacitor stability and control for more electric aircraft application. In *2020 European control conference (ECC)*.
Sabanovic, A., Fridman, L., & Spurgeon, S. (2004). *IEE control engineering series*: *Vol. 66*, *Variable Structure Systems: from Principles to Implementation*. IEE editor.
Sira-Ramírez, H. (2015). *Sliding mode control: The delta-sigma modulation approach*. Birkhäuser.
Sira-Ramírez, H., & Ilic, M. (1988). A geometric approach to the feedback control of switch mode DC-to-dc power supplies. *IEEE Transactions on Circuits and Systems*, *35*(10), 1291–1298.
Sira-Ramírez, H., & Silva-Ortigoza, R. (2006). *Power systems*, *Control design techniques in power electronic devices*. Springer.
Slotine, J., & Li, W. (1991). *Applied nonlinear control*. Prentice Hall.
Sun, L., Zhao, J., & Dimirovski, G. (2009). Nonlinear robust controller design for thyristor controlled series compensation. *International Journal of Innovative Computing, Information and Control*, *5*, 981–989.
Tooley, M. (2009). *Aircraft electrical and electronic systems: Principles maintenance and operation*. Butterworth-Heinemann.
Utkin, V. (1977). Variable structure systems with sliding modes. *IEEE Transactions on Automatic Control*, *22*(2), 212–222.
Utkin, V. (1992). *Sliding modes in control and optimization*. Springer Verlag.
Utkin, V. (1993). Sliding mode control design principles and applications to electric drives. *IEEE Transactions on Industrial Electronics*, *40*(1), 23–36.
Utkin, V. (1993). Sliding mode control design principles and applications to electric drives. *IEEE Transactions on Industrial Electronics*, *40*, 23–36.
Utkin, V., Guldner, J., & Shi, J. (2009). *Sliding mode control in electro-mechanical systems*. CRC Press.
Utkin, V., & Poznyak, A. (2013). Adaptive sliding mode control with application to super-twist algorithm: Equivalent control method. *Automatica*, *49*, 39–47.
Yang, Y., Zhong, W., Kiratipongvoot, S., Tan, S., & Hui, S. Y. R. (2018). Dynamic improvement of series compensated wireless power transfer systems using discrete sliding mode control. *IEEE Transactions on Power Electronics*, *33*(7), 6351–6360.
Young, K. D., Utkin, V. I., & Ozguner, U. (1999). A control engineer's guide to sliding mode control. *IEEE Transactions on Control Systems Technology*, *7*(3), 328–342.
Zhao, Y., Ma, D., & Zhao, J. (2018). L_2 bumpless transfer control for switched linear systems with almost output regulation. *Systems & Control Letters*, *119*, 39–45.
Zhao, Y., Zhao, J., Fu, J., & Dimirovski, G. M. (2019). Integrated h_∞ filtering bumpless transfer control for switched linear systems. *ISA Transactions*.

Alberto Cavallo is currently Full Professor both of Automatic Control at the University of Campania "Luigi Vanvitelli". His research interests deal with many aspects of the Theory of Automatic Control, including robust control techniques with aeronautic and aerospace applications, with parametric and uncertainties and H-2 and H-inf indices, high-order sliding manifold control, active control of sound and vibrations, modelling and control of smart actuators with hysteresis, and currently is working on energy management and supervisory control for More Electric Aircraft applications. He has published more than 120 journal and conference papers, and two books, one published by Springer and the other by Prentice Hall. Alberto Cavallo has been Coordinator and Principal Investigator of several International Research Projects on smart control of electric systems for innovative aeronautic applications.

Giacomo Canciello obtained the Laurea Degree (with Laude) at the former Second University of Napoli (currently, University of Campania "Luigi Vanvitelli") in 2014, discussing the Thesis "Identification and Vibration Control for Flexible Structures", advisor Prof. A. Cavallo. In 2018 he completed his Ph.D. in Automatic Control, discussing the Thesis "Sliding Manifold Control in Advanced Aeronautical Applications". His research interests include modelling, identification and control of vibrating systems and control of switching power system for aeronautic applications.

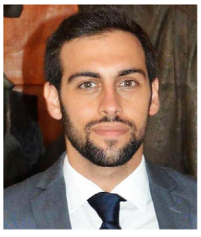

Antonio Russo received the Bachelor's and Master's degrees (with highest honours) in Computer Science Engineering from the University of Campania, "Luigi Vanvitelli", Aversa, Italy, in 2015 and 2017. He currently is a Ph.D. candidate in Automatic Control at University of Campania under the supervision of Professor Alberto Cavallo. From January 2019 to June 2019 he was a visiting Ph.D. student at University of Illinois at Urbana-Champaign under Professor Daniel Liberzon. His current research interests include nonlinear control, variable structure control of the sliding mode type, switched systems, control of power systems in the framework of the More Electric Aircraft.